Published in final edited form as:
J Nucl Med. 2017 October ; 58(10): 1666–1671. doi:10.2967/jnumed.117.192252.

18F--tetrafluoroborate (18F--TFB), a PET probe for imaging sodium-iodide symporter expression: Whole-body biodistribution, safety and radiation dosimetry in thyroid cancer patients

Jim O' Doherty[1], **Maite Jauregui-Osoro**[1], **Teresa Brothwood**[2], **Teresa Szyszko**[1], **Paul K. Marsden**[1], **Michael J. O' Doherty**[1], **Gary J. R. Cook**[1], **Philip J. Blower**[1], and **Val Lewington**[2]

[1]PET Imaging Centre, Division of Imaging Sciences and Biomedical Engineering, King's College London, St. Thomas' Hospital, London SE1 7EH, United Kingdom

[2]Department of Nuclear Medicine, Guy's & St. Thomas' Hospital NHS Foundation Trust, Great Maze Pond, London, SE1 9RT, United Kingdom

Abstract

Rationale—We report the safety, biodistribution and internal radiation dosimetry, in humans with thyroid cancer, of 18F-tetrafluoroborate (18F-TFB), a novel PET radioligand for imaging the human sodium/iodide symporter (hNIS).

Methods—Serial whole-body PET scans of 5 subjects with recently diagnosed with thyroid cancer were acquired prior to surgery for up to 4 hours after injection of 184 ± 15 MBq of 18F-TFB. Activity was determined in whole blood, plasma and urine. Mean organ absorbed doses and effective doses were calculated via quantitative image analysis and using OLINDA/EXM software.

Results—Images showed high uptake of 18F-TFB in known areas of high hNIS expression (thyroid, salivary glands and stomach). Excretion was predominantly renal. No adverse effects in relation to safety of the radiopharmaceutical were observed. The effective dose was 0.0326 ± 0.0018 mSv/MBq. The critical tissues/organs receiving the highest mean sex-averaged absorbed doses were thyroid (0.135 ± 0.079 mSv/MBq), stomach (0.069 ± 0.022 mSv/MBq) and salivary glands (parotids 0.031 ± 0.011 mSv/MBq, submandibular 0.061 ± 0.031 mSv/MBq). Other organs of interest were the bladder (0.102 ± 0.046 mSv/MBq) and kidneys (0.029 ± 0.009 mSv/MBq).

Corresponding author: Professor Val Lewington, M.D., Department of Nuclear Medicine, Guy's Hospital, Great Maze Pond, London, United Kingdom, val.lewington@gstt.nhs.uk, T: +44 (0) 20 7188 4112.
First Author:
Jim O' Doherty, PhD, PET Imaging Centre, King's College London, St. Thomas' Hospital, London SE1 7EH, United Kingdom, E: jim.odoherty@kcl.ac.uk, T: +44 (0) 20 7188 7446

Disclosure
This study was funded by an MRC Confidence in Concept grant administered by King's Health Partners. Financial support was also received from the Department of Health via the National Institute for Health Research (NIHR) comprehensive Biomedical Research Centre award to Guy's & St Thomas' NHS Foundation Trust in partnership with King's College London and King's College Hospital NHS Foundation Trust under grant number WT088641/Z/09/Z. Also supported by the Centre of Excellence in Medical Engineering Centre funded by the Wellcome Trust and EPSRC under grant number WT088641/Z/09/Z, and the King's College London and UCL Comprehensive Cancer Imaging Centre funded by CRUK and EPSRC in association with the MRC and DoH (England) (C1519/A16463).
The views expressed are those of the authors and not necessarily those of the NHS, the NIHR, the DoH, EPSRC or Wellcome Trust.

Europe PMC Funders Author Manuscripts

Conclusion—Imaging using 18F-TFB imparts a radiation exposure similar in magnitude to many other 18F--labeled radiotracers. 18F-TFB shows a similar biodistribution to 99mTc-pertechnetate, a known non-organified hNIS tracer, and is pharmacologically and radiobiologically safe in humans. Phase 2 trials as a hNIS imaging agent are warranted.

Keywords

18F-TFB; thyroid imaging; PET-CT

Introduction

The human Na^+/I^- symporter hNIS is a plasma membrane glycoprotein that mediates active I^- transport into thyroid epithelial and follicular cells. It also mediates transport of I^- into cells of other tissues that do not organify iodide, such as the salivary glands, gastric mucosa and breast (1). As a target for molecular imaging, its main clinical role has been in investigation of thyroid pathophysiology. Radioiodine has historically been used for both diagnostic thyroid imaging (using 123I-I^-) and to treat benign and malignant thyroid disease (using 131I-I^-) (2). Due to its similarity of volume and charge with iodide ions, 99mTc-$NaTcO_4^-$ (sodium pertechnetate) is also widely used to study thyroid function. To overcome the limitations of gamma camera planar and single photon emission tomography imaging with respect to resolution and senstivity, recent interest has focused on developing positron emission tomography (PET) tracers for thyroid imaging.

Phan *et al.* reported that 124I-I^- PET was a more sensitive diagnostic tool than 131I-I^- scintigraphy in 20 patients (3). A study by Gulec *et al.* with 124I-I^- PET identified 22.5% more iodine-avid foci than with planar 131I-I^- scintigraphy post-treatment (4). However, the complex decay scheme of iodine-124 (5) and low positron abundance result in poor PET imaging characteristics. Optimal target: background ratios are reported after 24 hours. It requires a complex cyclotron-based production and purification process (6) and due to its relatively long half-life of 4.2 days lead to a high effective dose (0.095-1.5 mSv/MBq) (7). Because of the superior PET-imaging characteristics and dosimetry of fluorine-18, a reliable and sensitive 18F-based radioligand for hNIS would have potential for molecular imaging of hNIS activity. Several small anionic species containing fluorine, such as tetrafluoroborate (BF_4^-), fluorosulfate (SO_3F^-), hexafluorophosphate (PF_6^-) and difluorophosphate ($PO_2F_2^-$) have been identified as hNIS substrates (8, 9). While 18F-SO_3F^- was only recently synthesized for the first time and shown to be an effective high-affinity NIS tracer in mice (10), the earliest reports of 18F-BF_4^- date from the 1960's (11–13). Our group recently developed a method for the synthesis of 18F-tetrafluoroborate (18F-TFB) suitable for routine clinical production, and showed it to be a tracer for hNIS, with similar biological behavior to 99mTc-TcO_4^- in vitro and in mice (14–16). Marti-Climent *et al.* detailed the characteristic biodistribution of 18F-TFB in NIS expressing tissues in cynomolgus primates, with uptake in the thyroid, stomach and salivary glands, and a mean whole body absorbed dose of 0.0247 mSv/MBq (17). Given the potential of an 18F-based radioligand for diagnosis and treatment planning in thyroid disease, we investigated the safety, biodistribution and radiation dosimetry 18F-TFB in a human population.

Europe PMC Funders Author Manuscripts

Materials & Methods

Radiopharmaceutical Preparation

Synthesis of the 18F-TFB IMP (Investigational Medicinal Product) was carried out by a method similar to a previously described automated labeling protocol (14) using an Eckert and Ziegler Modular-Lab synthesis unit (Imaging Equipment Ltd., Bristol, UK). 18F-fluoride (46 ± 6 GBq), obtained from proton-irradiated [^{18}O]water (98 atom%, Rotem Industries Ltd., Israel; 11 MeV protons from a CTI RDS 112 cyclotron, beam current 30 μA, irradiation time 60 min), was trapped in a QMA cartridge (Sep-Pak Light QMA cartridge, Waters, Elstree, UK) conditioned with 1.0 M sodium hydrogen carbonate (10 mL, Ph Eur, Merck) followed by water for injections (10 mL, BP, Hamelin Pharmaceuticals, Gloucester, UK) and air (10 mL). Hydrochloric acid (1.5 M, 1.2 mL), prepared by dilution of hydrochloric acid fuming 37% (Ph Eur, Merck) with water for injections (BP, Hameln Pharmaceuticals, Gloucester, UK), was then passed through the QMA cartridge, eluting the 18F-fluoride into the reactor which contained sodium tetrafluoroborate (Sigma-Aldrich, Gillingham, UK) (1 mg in 0.1 mL water for injections). The reaction mixture (1.3 mL) was heated to 80 °C for 15 min, cooled to 20 °C and passed through a silver ion-loaded cation exchange cartridge (OnGuard II AG, Dionex, Leeds, UK, conditioned with 10 mL water and 5 mL air) to remove chloride ions and raise the pH, and through two alumina cartridges (Waters SepPak Light Alumina N, conditioned with 10 mL water and 5 mL air) to remove unreacted 18F-fluoride. The product was eluted with water for injections (2 mL) into a nitrogen-filled USP type 1 glass sterile vial (N46, GE Healthcare) containing water for injections (2 mL). Following production, the vial containing the unfiltered product (5.3 mL) was transferred to a sterile isolator, for sterile filtration and quality control sampling. The process was validated to demonstrate that 18F-TFB can be consistently manufactured on the Modular-Lab synthesizer to meet the required quality control release specifications. Stability studies were conducted by testing an aliquot from the validation batches for radiochemical purity and pH at 2, 4 and 6 hours from end of synthesis.

Radiopharmaceutical quality control

Radiochemical identity, purity and specific activity of the final product were checked by ion chromatography (Metrohm 930 Compact IC Flex) with inline conductimetric and gamma detectors (B-FC-3200, LabLogic) using a Shodex IC I-524A column (4.6 × 100 mm) with 2.5 mM phthalic acid (adjusted to pH 4.0 with tris(hydroxymethyl)aminomethane) as eluent. The flow rate was 1.5 mL/min, and column temperature was 40 °C. The IC quality control method was validated following the International Conference on Harmonisation guidelines and the concentration of [$^{19/18F-}$] BF_4- in the final product was determined from the ion chromatogram by reference to a calibration curve. RadioTLC was carried out using a silica gel stationary phase (Silica gel 60 F_{254}, 5 × 10 cm, Merck) with methanol as the mobile phase. Plates were scanned using a radio-TLC scanner (LabLogic Scan-RAM) with a β^+ probe (PS Plastic-PM LabLogic). The radiochemical purity of the product was determined as the radioactivity associated with the tetrafluoroborate peak (*R*f = 0.6, c.f. *R*f = 0 for fluoride) as a percentage of the total chromatogram radioactivity. Silver content was determined using Quantofix Silver test strips (Macherey-Nagel). The bacterial endotoxin assay was performed using the Endosafe Portable Test System (Charles-River) using LAL

Europe PMC Funders Author Manuscripts

reagent water and licensed Endosafe Portable Test System cartridges (Charles River) with sensitivity of 0.05 - 5.0 EU/mL. The integrity of the sterilizing filters was tested after use using the bubble point method and sterility testing was carried out by Wickham Laboratories.

Patients

Patients were recruited in accordance with the European Council Directive. The clinical protocol was approved by the local Research Ethics Committee (reference number 14/LO/1247, ISRCTN: 75827286). All patients provided written informed consent.

Five subjects (2 male, 3 female, average age 46 years) with newly diagnosed, cytologically confirmed thyroid cancer were imaged prior to elective total thyroidectomy and 131I-NaI thyroid remnant ablation. Pregnant and lactating women were excluded.

A cannula was placed in a vein in the antecubital fossa of each arm, one for injection of 18F-TFB and the other for withdrawal of venous blood. Electrocardiographic monitoring, pulse, blood pressure, body temperature (using a temperature strip on the patient's forehead) and respiratory rate were monitored throughout the study.

PET-CT data acquisition

Bolus injection of 18F-TFB (mean 185 ± 15 MBq) was performed with the patient positioned on the scanning couch. Imaging comprised a 90-minute series of 7 sequential whole body PET–CT scans (from head to foot), followed by 2 further whole body PET-CT scans at 120 and 240 minutes post-injection (see Figure 1) with a GE Discovery 710 PET-CT scanner (GE Healthcare, Waukesha, USA) with an axial field of view of 15.7 cm. Each scan covered the vertex to midthigh, with an 11-slice overlap between bed positions. Three low-dose whole body CT scans (140 kV, 10 mA, 0.5 s rotation time, 40 mm collimation) were performed, one prior to the block of 7 sequential scans and then one prior to each of the scans at 120 and 240 minutes, for attenuation correction and anatomical reference. The initial 1 minute per bed scan duration was adjusted to compensate for radioactive decay up to a maximum of 3 minutes/bed step for the final scan at 240 min.

Quantification of blood and urine data

Venous blood samples (5 mL each) were acquired at 0, 1, 2, 5, 10, 20, 40, 60, 90, 120 and 240 minutes post injection. Three 0.2 mL aliquots from each blood sample were weighed and counted on a 10-sample well counter (2470 WIZARD2, PerkinElmer, London, UK), previously cross-calibrated with fluorine-18 to the PET scanner using a standard calibration technique subject to daily quality control. Whole blood samples were centrifuged for 5 minutes (6000 rpm), and three 0.2 mL samples of plasma from each were then counted in the well counter. Following the method of Namias *et al.* (18), the distribution ratio $R(t)$, between blood cells and plasma can be calculated from experimental measurements of the whole blood and plasma activity concentrations (C_{WB} and C_P respectively) at each time point using the equation:

$$R(t) = C_{BC}(t)/C_P(t) \quad [1]$$

where the blood cell activity concentration, $C_{BC,}$ can be calculated from:

$$C_{BC}(t) = \frac{C_{WB}(t) - (1 - H)C_P(t)}{H} \quad [2]$$

The value H represents hematocrit (assumed for each patient as H=0.39). Before application of equations [1] and [2], C_{BC} and C_P were expressed in Bq/kg of water, assuming that plasma contains 0.94 kg water/L and erythrocytes contain 0.73 kg/L (19).

Urine was collected as voided in the intervals between imaging (i.e. between 90-120 minutes and 140-260 minutes), weighed for total excreted volume, and three aliquots (0.2 mL each) of each void were used to determine the total excreted activity of 18F-TFB.

Image Reconstruction

Each whole body PET image was attenuation-corrected using its corresponding CT image and included standard scanner-based corrections for decay, scatter, randoms and dead-time. Each emission scan was reconstructed with a time-of-flight OSEM algorithm (2 iterations, 24 subsets), into a 256x256 matrix. A 4 mm full width at half maximum Gaussian post-reconstruction smoothing filter was applied. Accuracy of the activity in the PET images was verified by summing the activity in the first whole-body PET scan and comparing with the decayed injected activity.

Absorbed dose calculations

Whole body CT images from the 120 and 240 min PET-CT scans were rigidly registered to the 0-90 min CT using the PFUS package of PMOD v3.7 (PMOD Technologies, Zurich, Switzerland). The resulting transformations were then applied to the corresponding PET images. All PET frames were then merged to a single 4D series decay-corrected to a common time point. Organs of interest were identified and manually delineated by an experienced clinician using a fusion of both the corresponding CT and PET images. A software correction was included to account for the imaging time of each bed position in the WB sweeps. Visible organs with high uptake or easily identified on CT imaging were the brain, thyroid, liver, spleen, stomach, heart, kidneys, lungs, testes (male only) and urinary bladder contents. Organ volumes were transferred to all frames and independent volumes were adjusted where necessary to account for any movement of organs between different frames. All organs with the exception of the bladder were assumed to have a constant volume over time. The volume of the bladder was quantified on each PET scan using a 25% of maximum isocontour. PMOD software allows the automatic naming and standardized volume determination of each organ relating to the 70 kg Cristy-Eckerman adult anthropomorphic phantom employed by OLINDA/EXM (Organ Level Internal Dose Assessment/Exponential Modeling) dose calculation software, a software package widely

used to obtain radiation dose estimates in radiopharmaceutical studies (20). Time-activity curves (TACs) were produced for each organ, and using the PKIN package of PMOD v3.7. Organ 'normalized cumulated activities' (NCA – numerically equivalent to the older terminology of 'residence time' measured in MBq.h/MBq) were automatically calculated using the net injected activity and organ volume. TACs were fitted to bi-exponential functions where possible, assuming radionuclide decay (i.e. no further excretion) upon reaching the last imaging point. Mean blood activity concentration was generated in calibrated kBq/mL from the average value of the three samples. Total blood activity was calculated assuming 5.4% of the reference phantom's mass (70 kg) was blood. The blood TAC was fitted with an exponential curve, the NCA determined and this value used as the NCA for the red marrow in OLINDA calculations.

Summed activities of the urinary bladder and voided urine over the course of the study were fitted with a 1-phase exponential curve using the formula:

$$U(t) = U_{\max} \times \left[1 - \exp\left(-\ln 2 \times \frac{t}{T_{\frac{1}{2}}}\right)\right] \quad [3]$$

where $U(t)$, U_{max} and $T_{1/2}$ represent the accumulated urine activity at time t, maximum accumulated urine activity and biological half-life respectively. From the fitting parameters, U_{max} and $T_{1/2}$ were determined and the NCA of the urinary bladder contents was calculated using a dynamic urinary bladder model in the OLINDA/EXM v1.1 software. A 3.5 hour voiding interval was used as recommended by the ICRP (21). The "remainder of body" was assigned by activity not accounted for by organ delineation or excretion. Effective doses according to the tissue weighting factors of ICRP Publication 60 in each organ were calculated by inputting calculated NCAs into OLINDA/EXM. Absorbed doses to the 24 organs specified by the Medical Internal Radiation Dose scheme in the target organs of the Cristy-Eckerman adult hermaphrodite male and female phantoms were determined, and sex-specific absorbed doses were averaged. Gonad absorbed dose was taken to be the mean of the absorbed doses to the testes and ovaries. Absorbed doses to the salivary glands, which are not assigned organs in the OLINDA/EXM scheme, were also investigated. The submandibular and parotid glands were assigned a mass of 9.9 g and 18 g respectively with a density of 1 cm^3/g (values previously used for salivary gland dosimetric purposes (22)). NCAs for each gland from imaging were inputted into the "Spheres" module of the OLINDA/EXM software, and a curve of the form $d = a \times m^b$ was fitted to the resulting dose (mGy/MBq) to mass (g) relationship to determine the dose at the mass of the gland under investigation.

Results

Safety

In all 18F-TFB batches, radiochemical purity was > 99.8% as shown by radio-IC and radio-TLC, no silver was detected, radionuclidic purity was 100% and no impurities were found.

All batches were sterile and pyrogen free. The mean and standard deviation of the administered mass of 19F/18F-TFB was 9 ± 4 μg and the specific activity at the time of injection was 24 ± 13 MBq/μg. 18F-TFB was found to be safe and well-tolerated by all patients. There were no adverse or clinically detectable pharmacologic effects in any of the 5 subjects. No significant changes in vital signs or electro- cardiograms were observed.

Biodistribution

Figure 2 shows the biodistribution of 18F-TFB over time for a single representative patient. All patients showed similar biodistribution characteristics. The thyroid is clearly visible from the earliest time point, with uptake reaching a peak at approximately 30 minutes post-injection for all patients. Outside the thyroid, reconstructed images show high uptake in other areas of elevated hNIS expression, such as the salivary glands and stomach. Excretion was primarily renal. Esophageal transit of 18F-TFB can be observed at later time points as saliva generated in the salivary glands is swallowed and enters the stomach and intestinal system. The oral cavity also shows increased activity 1 hour post-injection, probably due to pooling of saliva. Images show low uptake in areas that do not significantly express hNIS, such as the brain and liver. Tumour nodules ranging in size from 13 – 114mm maximum diameter are photopaenic against background healthy thyroid 18F-TFB uptake, consistent with lower hNIS expression in DTC relative to normal thyroid. Persisting low intensity blood pool activity was observed on delayed images.

Figure 3 shows the average percent of injected activity over all patients for a range of organs considered for dosimetric purposes while Figure 4 details the plasma and blood activity concentrations as well as the distribution ratio of the radiotracer.

Radiation Dosimetry

Using TACs derived from biodistribution imaging, the absorbed doses per unit administered activity to the Medical Internal Radiation Dose scheme listed organs, as determined from OLINDA and averaged over all patients, are provided in Table 1. The highest absorbed organ doses were those to the thyroid, stomach and bladder.

Discussion

This work presents the first study of the biodistribution and radiation dosimetry of 18F-TFB in humans. Previous work in primates (also using OLINDA and assuming distribution in the Cristy-Eckerman phantom) demonstrated a whole body absorbed effective dose of 0.0247 ± 0.0028 mSv/MBq, which compares well with our calculated value of 0.0326 ± 0.0018 mSv/MBq averaged over men and women, despite physiological differences between humans and primates. As evident in Figure 2, organs with highest tracer uptake correspond to tissues associated with high hNIS expression. Increased uptake in the stomach reflects a combination of hNIS expression and swallowed saliva, following secretion by the salivary glands. Images are consistent with 18F-TFB passing from the salivary glands into the mouth and through the esophagus into the stomach. The average mass of tetrafluoroborate injected (9 μg) corresponds to approximately 0.1 μmol, which assuming a total extracellular fluid volume (including plasma) of 15 L would lead to a maximum concentration of

tetrafluoroborate in extracellular fluid of around 7 nM, much lower than the range of values reported for the IC50 of tetrafluoroborate (ca. 1 μM) (10). Therefore it is unlikely that significant blocking of hNIS occurs in these studies despite reported concerns (15).

The large standard deviations observed in the organs and tissues with high hNIS expression, such as the thyroid and salivary glands, show that uptake in these tissues is variable amongst the small population studied. As detailed in Figure 4, blood and plasma sample counting shows that 18F-TFB equilibrates between plasma and blood cells, with the distribution ratio converging to a constant value of approximately 0.74 by 30 minutes.

Matched radionuclide pairs for diagnostic imaging and radionuclide treatment are an integral part of nuclear medicine and the field has attracted the name "theranostics". 99mTc-TcO_4^- is often used to estimate accumulation and trapping function prior to $131I^-$ treatment of hyperthyroidism (23), the pattern and intensity of 99mTc-TcO_4^- uptake indicating the aetiology of hyperthyroidism (Grave's disease, multinodular goiter, thyroiditis). Comparisons have shown good imaging concordance between radioiodine and 99mTc-TcO_4^- (24, 25). Like 99mTc-TcO_4^-, 18F-TFB is trapped but not organified by the thyroid. Further investigation of its potential as a diagnostic in hyperthyroidism and comparison with 99mTc-TcO_4^- are warranted. 18F-TFB may have applications for TSH stimulated detection of differentiated thyroid cancer metastases following surgery and thyroid remnant ablation as an imaging partner for 131I-I^- therapy. By comparison with I^-124 I^-PET, 18F-TFB offers a low absorbed dose and favorable imaging characteristics that allow early imaging by comparison with I-124 I^- PET. 18F-TFB may also have potential for the investigation of other hNIS expressing tumour types such as breast and salivary gland cancers.

There are limitations with assuming organs and tissues as unit density spheres as employed here for calculation of radiation doses to organs not present in the OLINDA models, with some reports showing differences in radiation dose of over 100% between this method and "gold standard" Monte Carlo simulations (26). These differences mainly arise due to differences in tissue geometry compared to a true sphere. Although the unit density spheres model is only an approximation to clinical reality, our results are on the same order as previous works in primates, which also used the same methodology for calculation of the salivary gland doses (17) (literature values: parotid:0.0413 mGy/MBq; submandibular gland: 0.0274 mGy/MBq).

In comparison to other commonly used radiotracers employed in thyroid imaging, Table 2 shows that 18F-TFB delivers a much lower absorbed radiation dose than the radioiodine family of tracers for both medium and high levels of thyroid uptake. Image quality within 1 hour of administration (mean administered activity 185 MBq) was consistently excellent in this pilot study. Future studies may be able to optimize the injected activity.

Conclusion

18F-TFB is a hNIS substrate analogous in biodistribution to 99mTc-pertechnetate and is taken up selectively in hNIS-expressing tissues. It is safe to administer in humans and its

biodistribution and dosimetry warrant further clinical evaluation as a PET tracer for imaging thyroid pathophysiology and hNIS expression.

Acknowledgements

The authors thank the radiography staff at the PET Centre at St Thomas' Hospital for their help in collecting the data and radiochemistry staff for radiotracer production.

References

1. Chung J-K. Sodium iodide symporter: its role in nuclear medicine. J Nucl Med. 2010; 43:1188–1200.
2. Silberstein EB, Alavi A, Balon HR, et al. The SNMMI practice guideline for therapy of thyroid disease with ^{131}I 3.0. J Nucl Med. 2012; 53:1633–1651. [PubMed: 22787108]
3. Phan HT, Jager PL, Paans AM, et al. The diagnostic value of ^{124}I-PET in patients with differentiated thyroid cancer. Eur J Nucl Med Mol Imaging. 2008; 35:958–965. [PubMed: 18175115]
4. Gulec SA, Kuker RA, Goryawala M, et al. ^{124}I PET/CT in patients with differentiated thyroid cancer: Clinical and quantitative image analysis. Thyroid. 2016; 26:441–448. [PubMed: 26857905]
5. Woods DH, Woods SA, Woods MJ, et al. The standardization and measurement of decay scheme data of ^{124}I. Int J Radiat Appl Instrum Part A Appl Radiat Isot. 1992; 43:551–560.
6. Schmitz J. The production of [^{124}I]iodine and [^{86}Y]yttrium. Eur J Nucl Med Mol Imaging. 2011; 38(Suppl 1):S4–9. [PubMed: 21484376]
7. Johansson L, Mattsson S, Nosslin B, Leide-Svegborn S. Effective dose from radiopharmaceuticals. Eur J Nucl Med. 1992; 19:933–938. [PubMed: 1308762]
8. Anbar M, Guttman S, Lewitus Z. Effect of monofluorosulphonate, difluorophosphate and fluoroborate ions on the iodine uptake of the thyroid gland. Nature. 1959; 183:1517–1518. [PubMed: 13666792]
9. Waltz F, Pillette L, Ambroise Y. A nonradioactive iodide uptake assay for sodium iodide symporter function. Anal Biochem. 2010; 396:91–95. [PubMed: 19733144]
10. Khoshnevisan A, Chuamsaamarkkee K, Boudjemeline M, et al. ^{18}F-fluorosulfate for PET imaging of the sodium/iodide symporter: synthesis and biological evaluation in vitro and in vivo. J Nucl Med. 2017; 58:156–161. [PubMed: 27539841]
11. Anbar M, Inbar M. The application of F18 labelled fluoroborate ions to problems in thyroid physiology. Israel Atomic Energy Commission; 1962.
12. Askenasy HM, Anbar M, Laor Y, Lewitus Z, Kosary IZ, Guttmann S. The localization of intracranial space-occupying lesions by fluoroborate ions labelled with fluorine 18. Am J Roentgenol Radium Ther Nucl Med. 1962; 88:350–354.
13. Entzian W, Aronow S, Soloway AH, Sweet WH. A preliminary evaluation of F-18-labelled tetrafluoroborate as a scanning agent for intracranial tumors. J Nucl Med. 1964; 5:542–550. [PubMed: 14216632]
14. Jauregui-Osoro M, Sunassee K, Weeks AJ, et al. Synthesis and biological evaluation of [^{18}F]tetrafluoroborate: a PET imaging agent for thyroid disease and reporter gene imaging of the sodium/iodide symporter. Eur J Nucl Med Mol Imaging. 2010; 37:2108–2116. [PubMed: 20577737]
15. Khoshnevisan A, Jauregui-Osoro M, Shaw K, et al. [^{18}F]tetrafluoroborate as a PET tracer for the sodium/iodide symporter: the importance of specific activity. EJNMMI Res. 2016; 6:34. [PubMed: 27103614]
16. Weeks AJ, Jauregui-Osoro M, Cleij M, Blower JE, Ballinger JR, Blower PJ. Evaluation of [^{18}F]-tetrafluoroborate as a potential PET imaging agent for the human sodium/iodide symporter in a new colon carcinoma cell line, HCT116, expressing hNIS. Nucl Med Commun. 2011; 32:98–105. [PubMed: 21085047]

17. Martí-Climent JM, Collantes M, Jauregui-Osoro M, et al. Radiation dosimetry and biodistribution in non-human primates of the sodium/iodide PET ligand [^{18}F]-tetrafluoroborate. EJNMMI Res. 2015; 5:1–9. [PubMed: 25853007]

18. Nahmias C, Wahl LM, Amano S, Asselin M-C, Chirakal R. Equilibration of 6-[^{18}]fluoro-L-m-tyrosine between plasma and erythrocytes. J Nucl Med. 2000; 41:1636–1641. [PubMed: 11037992]

19. Siggaard-Andersen O. The acid-base status of the blood. 4th ed. Copenhagen: Munksgaard; 1976.

20. Stabin MG, Sparks RB, Crowe E. OLINDA/EXM: the second generation personal computer software for internal dose assessment in Nuclear Medicine. J Nucl Med. 2005; 46:1023–1027. [PubMed: 15937315]

21. Internation Commission on Radiological Protection. ICRP publication 56, part 2: Age- dependent doses to members of the general public from intake of radionuclides. Ann ICRP. 1992; 20

22. Jentzen W, Hobbs RF, Stahl A, Knust J, Sgouros G, Bockisch A. Pre-therapeutic ^{124}I PET(/CT) dosimetry confirms low average absorbed doses per administered ^{131}I activity to the salivary glands in radioiodine therapy of differentiated thyroid cancer. Eur J Nucl Med Mol Imaging. 2010; 37:884–895. [PubMed: 20069293]

23. Sucupira MS, Camargo EE, Nickoloff EL, Alderson PO, Wagner HNJ. The role of ^{99m}Tc pertechnetate uptake in the evaluation of thyroid function. Int J Nucl Med Biol. 1983; 10:29–33. [PubMed: 6305864]

24. Reschini E, Catania A, Ferrari C, Bergonzi M, Paracchi A, Raineri P. Comparison of pertechnetate and radioiodine thyroid scintiscans in thyroid disease. J Nucl Biol Med. 1993; 37:12–17. [PubMed: 8392382]

25. Krishnamurthi GT, Shoop L, Walsh C, Blahd WH. Comparison of 99mtechnetium pertechnetate and radioiodine (I-131) as thyroid Scanning Agents. Nuklearmedizin. 1973; 1973:97–106.

26. O'Doherty J, Clauss R, Scuffham J, Khan A, Petitguillaume A, Desbree A. Three dosimetry models of lipoma arborescens treated by ^{90}Y synovectomy. Med Phys. 2014; 41:052501. [PubMed: 24784398]

27. Department of Health. , editorAdministration of Radioactive Substances Advisory Committee. ARSAC Notes for Guidance: good clinical practice in nuclear medicine. Notes for Guidance on the Clinical Administration of Radiopharmaceuticals and use of sealed Radioactive SourcesLondon UK: 2016.

28. Mattsson S, Johansson L, Leide-Svegborn S, et al. Radiation Dose to Patients from Radiopharmaceuticals: A Compendium of Current Information Related to Frequently Used Substances. Ann ICRP. 2015; 44(2S) International Commission on Radiological Protection. ICRP publication 128.

29. Delbeke D, Coleman RE, Guiberteau MJ, et al. Procedure guideline for tumor imaging with ^{18}F-FDG PET/CT 1.0*. J Nucl Med. 2006; 47:885–895. [PubMed: 16644760]

Europe PMC Funders Author Manuscripts

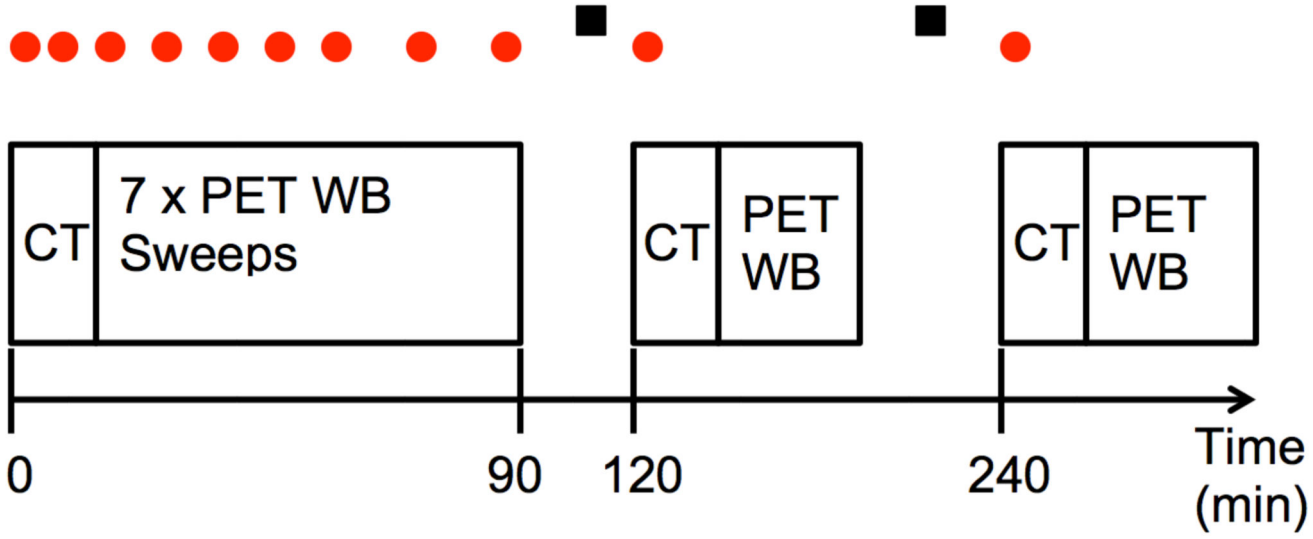

Figure 1.

Imaging scan schedule for the whole-body dynamic PET-CT study (not to scale). Dots above the scan positions show the timings of venous blood sampling and squares represent nominal urine sampling times.

Europe PMC Funders Author Manuscripts

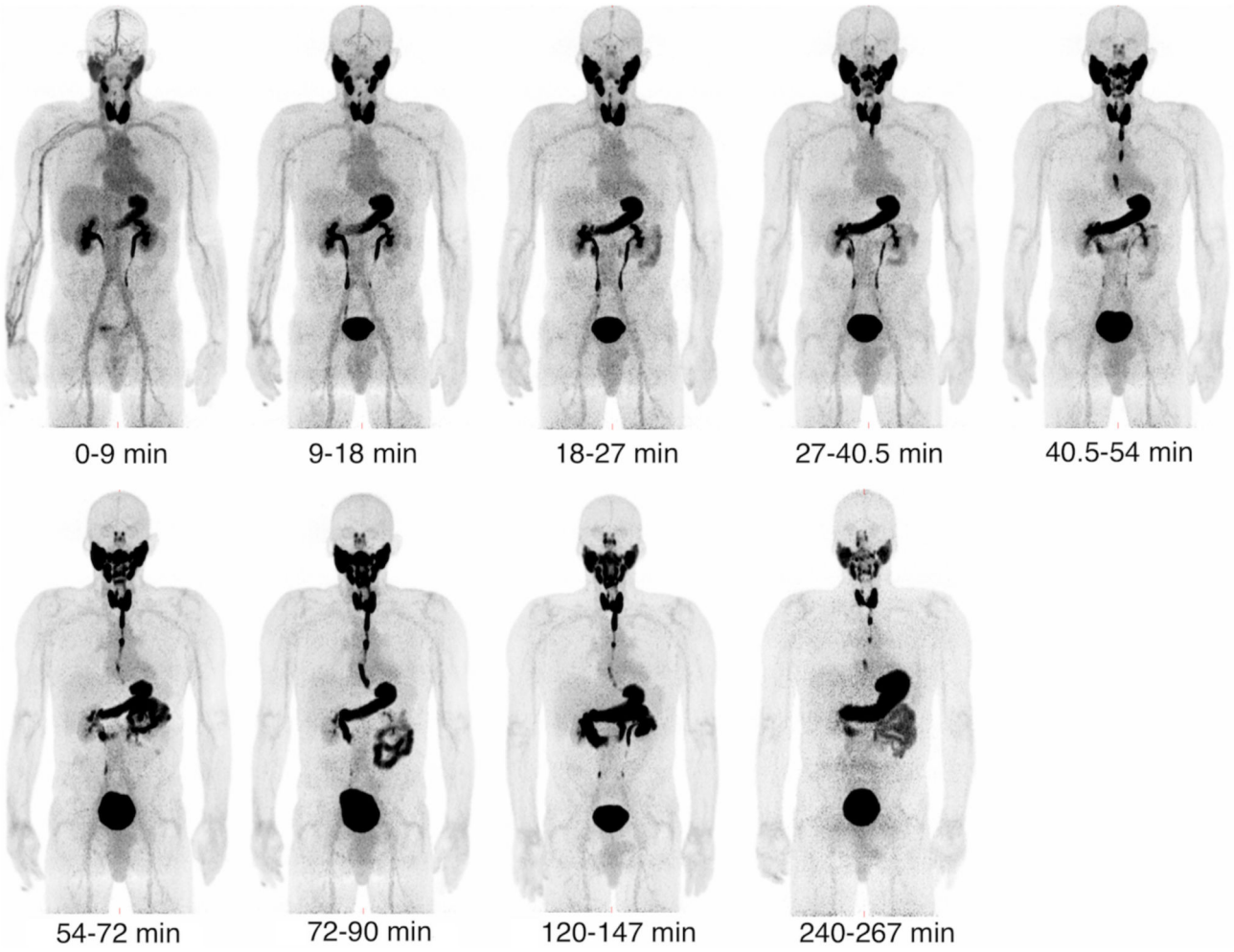

Figure 2.

Decay-corrected serial maximum-intensity projections showing the biodistribution of 18F-TFB over the course of the imaging study. Thyroid, salivary gland and stomach activities increase rapidly with time up to 30 minutes. Image captioned t = 0-9 min represents the first imaging frame.

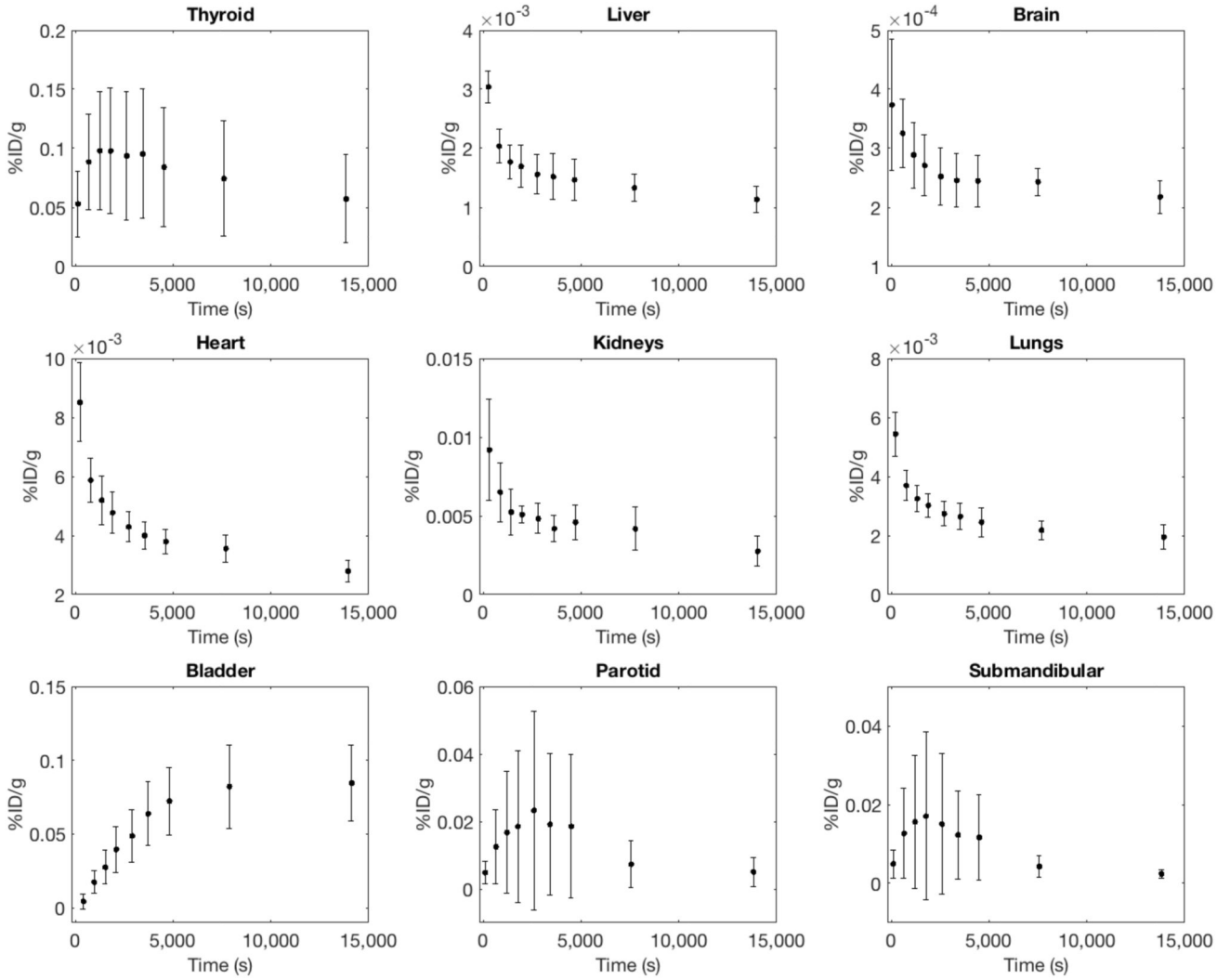

Figure 3.

Percentage of injected dose per gram of tissue (%ID/g) curves for selected organs, averaged over all 5 patients. Large standard deviations are evident in the hNIS expressing tissues and organs

Europe PMC Funders Author Manuscripts

Europe PMC Funders Author Manuscripts

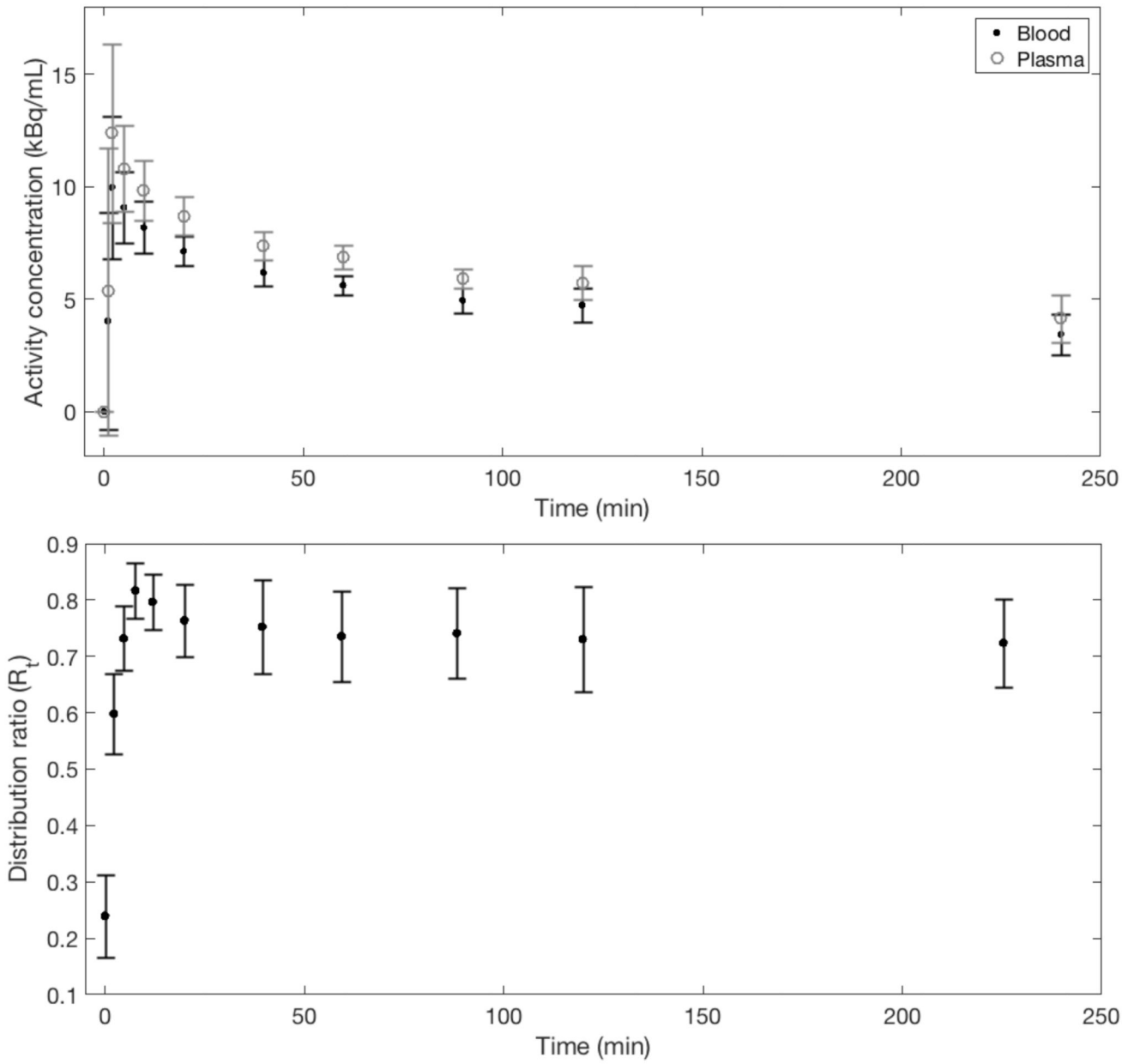

Figure 4.

Top - Mean decay-corrected blood and plasma curves averaged over all 5 patients. Bottom - mean blood cells to plasma distribution ratio, showing that equilibrium is reached after approximately 30 minutes. Error bars in both plots represent 1 standard deviation of the mean.

Europe PMC Funders Author Manuscripts

Table 1

Radiation absorbed doses for organs identified in the Medical Internal Radiation Dose schema. * Denotes organs that are not in the OLINDA model, with absorbed dose (in mGy/MBq) estimated from the "Spheres" model within the OLINDA/EXM software.

Organ/Tissue	Mean (mSv/MBq)	Std. dev. (mSv/MBq)
Gonads	0.020	0.014
Adrenals	0.015	0.003
Brain	0.005	0.001
Breasts	0.009	0.003
Gallbladder Wall	0.015	0.004
LLI Wall	0.016	0.004
Small Intestine	0.014	0.003
Stomach Wall	0.069	0.022
ULI Wall	0.014	0.004
Heart Wall	0.018	0.004
Kidneys	0.029	0.009
Liver	0.018	0.004
Lungs	0.011	0.003
Muscle	0.011	0.003
Pancreas	0.018	0.004
Marrow	0.034	0.003
Osteogenic Cells	0.033	0.005
Skin	0.008	0.002
Spleen	0.020	0.003
Thymus	0.011	0.003
Thyroid	0.135	0.079
Urinary Bladder wall	0.102	0.046
Uterus	0.019	0.004
Total Body	0.011	0.003
*Parotid	0.031	0.011
*Submandibular	0.061	0.031
Effective Dose	**0.0326**	**0.0018**

Europe PMC Funders Author Manuscripts

Table 2

Comparison of the whole body effective doses in mSv/MBq for a range of radiotracers utilized for imaging of the thyroid. All values except 18F-TFB are from ICRP Publication 128 (28). FDG value from (29).

Radiopharmaceutical	Effective dose (mSv/MBq)	Nominal Imaging Activity (MBq)(27)
131I-I^-	22 *, 29 †	3-10
[^{123}I]I^-	0.23 ≠ 0.31 §	20
[^{124}I]I^-	13 ≠, 18 §	50
99mTc-TcO_4^-	0.013 ∥	80
18F-TFB	0.0289	200
18F-FDG	0.019	400

* medium thyroid uptake, no blocking, oral admin, adult

† high thyroid uptake, no blocking, oral admin, adult

≠ medium thyroid uptake, no blocking, IV admin, adult

§ high thyroid uptake no blocking, IV admin, adult

∥ IV administration, adult